JOURNAL OF MATERIALS SCIENCE 31 (1996) 4159–4164

The effect of carbon containing atmosphere on the structure and mechanical properties of Fe–32Mn–9.4Al–1C–1.27Si alloy

J. Y. LIU, S. C. CHANG
Institute of Materials Science and Engineering, National Tsing Hua University, Hsinchu, Taiwan

The effect of a carbon containing atmosphere on the microstructure and mechanical properties of Fe–32Mn–9.4Al–1C–1.27Si alloy was investigated in this work. Surface oxide nodules and grain boundary oxides were found to form on this alloy when it was annealed in carbon-containing air at 1050 °C for 1 h. The oxidation reaction was thought to be the result of the "green rot" attack process. This alloy was embrittled severely by the carbon-containing air through the formation of surface oxide nodules and grain boundary oxide. The carbon-containing air enhanced the oxidation rate of this alloy at 1050 °C. The structure of the oxide nodules formed on this alloy in the carbon-containing air was similar to that observed on a FeMnAl alloy heated in 1000 °C air for 24 h.

1. Introduction

FeMnAl alloys have attracted a lot of researchers' attention with respect to their mechanical properties [1–5], oxidation behaviour [6–10], corrosion properties [11–17], and phase transformation behaviour [4, 18–20] in the past ten years. The corrosion resistance of the austenitic structure of FeMnAl was found to be superior to that of the ferrite structure in NaCl solution and molten salts [21–23]. But fully ferritic FeMnAl alloy was reported to be more oxidation resistant than austenitic FeMnAl alloy in a pure oxygen atmosphere [7–8]. The difference in oxidation resistance between ferritic and austenitic FeMnAl alloys was attributed to the ease of forming a protective Al_2O_3 layer on the ferritic FeMnAl alloy's surface. Adding Si to the FeMnAl alloy had been reported to be capable of improving the strength, corrosion resistance, and high temperature oxidation resistance of FeMnAl alloys [1, 2, 6, 12, 13, 24].

Interaction of constructional materials with the environment is one of the major stages of structure degradation encountered in industry. Corrosive aqueous solutions, molten salts, air, and carbon-containing gases are the most common environments which cause the degradation of constructional materials. FeMnAl alloy is a newly designed alloy system. A study of the interaction of FeMnAl alloy with these environments will be helpful in the application of this alloy system. Carbon-containing gas is a general material-destructive environment in the petroleum industry. It causes tremendous monetary loss through the degradation of production facilities every year. Although a lot of studies have been conducted to understand the corrosion, oxidation and nitriding properties of FeMnAl alloys, the behaviour of FeMnAl alloy in a carbon-containing gas has not been studied yet. This work tries to clarify the behaviour of Fe–32Mn–9.4Al–1C–1.27Si alloy annealed in a carbon-containing gas at 1050 °C. A comparison of microstructural and mechanical properties of this alloy exposed to both air and carbon-containing gases is also given.

2. Experimental procedure

The chemical composition of the alloy studied in this work is as follows:

element	Fe	Mn	Al	C	Si
wt %	bal.	32	9.36	1	1.27

This alloy was prepared by melting electrolytic iron, aluminium, manganese, silicon, and pure carbon powder in a laboratory induction furnace. The cast ingot was hot rolled to a 15 mm plate at 1200 °C, water quenched, and then homogenized at 1150 °C for 0.5 h or 1100 °C for 12 h. After homogenization, the hot-rolled plate was machined with a planer to remove the oxide scale and surface layer where phase transformation might have occurred during homogenization. 5 mm of thickness was removed from the hot-rolled plate by this planing process. The machined plate was then cold rolled to 3 mm and solution annealed. The cold-rolled plate homogenized at 1150 °C was solution annealed at 1150 °C and that homogenized at 1100 °C was solution annealed at 1050 °C. G represented the homogenizing process at 1150 °C for 0.5 h and solution annealing in air at 1150 °C for 5 minutes. Gl represented the homogenizing process at 1100 °C for 12 h and solution annealing in carbon-containing gas, which was generated by the coexistence of air and

0022–2461

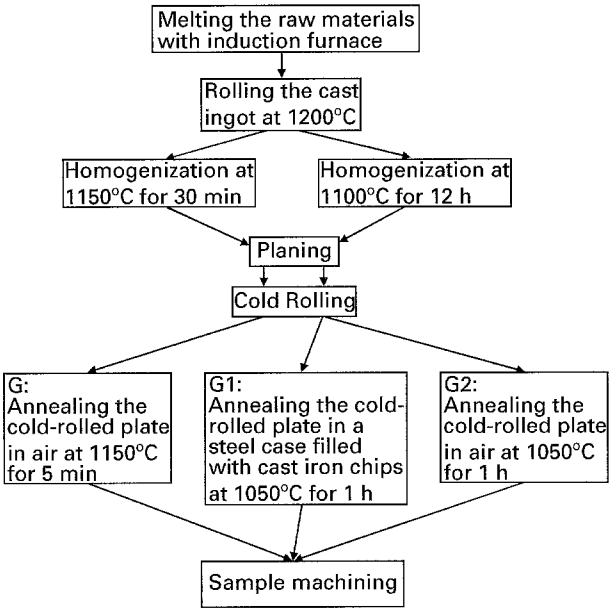

Figure 1 Flow chart of sample preparation process.

cast iron chips in a steel casing, at 1050 °C for 60 min. G2 represented the homogenizing process at 1100 °C for 12 h and solution annealing in air at 1050 °C for 60 min. The treatment processes employed in this work are illustrated in Fig. 1.

Microstructure and tensile properties of this alloy were studied after solution annealing. The microstructures were examined by optical microscopy (OM) and identified by X-ray diffraction (XRD). Energy dispersive X-ray spectrometry (EDS) was also adopted for analysing the chemical composition of the structure which cannot be identified by X-ray diffraction. Tension test specimens were prepared according to the ASTM standard. They were ground with SiC paper after machining off the black surface oxide layer generated during solution annealing. About 150 μm thickness was ground off from every specimen. After tensile testing, the fracture surface of each specimen was examined by scanning electron microscopy (SEM).

3. Results

3.1. Microstructure

The bulk structure of Fe–32Mn–9.4Al–1C–1.27Si alloy was austenite despite the treating process. Fig. 2a shows a typical microstructure photograph of this alloy and Fig. 2b gives its X-ray diffraction pattern. Interaction of the alloy with the annealing environment only changed the microstructure of the surface portion of this alloy. When treating this alloy using the G process, only a thin black oxide scale (less than 10 μm thick) was formed on the surface of this alloy. Ferrite phase and a thin black oxide layer were observed on the alloy when it was treated by the G2 process. The thickness of the two-phase region was in the range 100 to 300 μm, as shown in Fig. 3b. Two kinds of surface microstructure were observed on the specimen treated by the G1 process. As the cast iron chips filled the heat-treatment container and covered the specimen completely, only the thin black scale was observed on the resultant specimen just like that which occurred on the specimen treated by the G process. When the cast iron chips did not fill the heat-treatment container and air was present, nodules of a needle-like structure formed on the specimen as shown in Fig. 3d. Additionally, a coarse grain boundary region, extending over more than four grains below the nodule structure, was also observed.

3.2. Tensile test

Table I gives the tensile test results of the Fe–32Mn–9.4Al–1C–1.27Si alloy treated with G, G1, and G2 processes. This alloy fractured in a typical ductile mode and its elongation was greater than 50% when it was treated by either the G or G2 process. But it fractured in both ductile and brittle modes when it was treated by the G1 process. Brittle fracture only occurred on the specimen containing the needle-like phase. The elongation of the brittle-fractured specimens varied from 16 to 55% depending on the volume fraction of the needle structure. The brittle-fractured crack propagated transgranularly through the grain with the needle-like structure and then along the coarse grain boundary as shown in Fig. 4. The alloy's strength and elongation increased with decreasing thickness of the needle-like structure and coarse grain boundary region. Finally, it fractured in ductile mode when the needle-like structure and coarse grain boundary were removed completely. The alloy's tensile strength was greater than 800 MPa regardless of the annealing process. The ranking of the tensile strength of this alloy treated by these three processes was G > G1 > G2.

3.3. Phase identification

Fig. 5 is the X-ray diffraction pattern of the needle-like structure. This structure is shown to be a mixture of Al_2MnO_4 and AlN. Since the volume of the coarse grain boundary was too small to be identified by X-ray diffraction, EDS analysis was conducted to obtain its chemical composition. Fig. 6 gives the locations of EDS analysis and the corresponding spectrum pattern. An oxygen peak was observed in the EDS spectrum of the coarse grain boundary as shown in Fig. 6b. It indicated that the coarse grain boundary (G.B.) was also an oxide. The chemical compositions of the coarse grain boundary are as follows:

	Fe	Mn	Al	Si
Coarse G.B.	58.00	30.67	10.19	1.15
Location B	59.69	31.87	7.74	0.69

Location B is the site beside the coarse grain boundary. In addition to the oxygen peak, the EDS analysis shows that the Al and Si content in the region beside the coarse grain boundary is somewhat depleted.

4. Discussion

Oxidation of FeMnAlSi in air at temperatures $\geqslant 1000$ °C has been observed to proceed by the formation of oxide nodules and the overgrowth of

these oxide nodules to cover the alloy's surface [25]. The oxidation reaction was thought to be accomplished by the diffusion of Mn outward and oxygen inward [6]. The observed thin black scale and the two-phase region ($\alpha + \tau$) on the Fe–32Mn–9.4Al–1C–1.27Si alloy annealed by the G2 process were the products of the interaction of this alloy with air at this high temperature. Mn and C act as austenite structure stabilizers in FeMnAl alloy. Since oxidation of this alloy was accomplished by the outward diffusion of Mn, the formation of ferrite grains would result from the depletion of Mn in the surface region. On the other hand, the movement of carbon atoms in the metal at 1050 °C is easy. Heating this alloy in air at 1050 °C, carbon atoms might diffuse outward to the alloy's free surface and react with the oxygen in the air to form CO_2. As for the Mn depletion condition, carbon in the surface region would also be depleted through the diffusion and oxidation reaction. This process would enhance the ferrite formation reaction. That no α-phase was observed in this alloy when annealed in air at 1150 °C for 5 min (G process) might result from the short heating time interval.

Heating this alloy in a carbon-containing atmosphere, which was generated by the coexistence of air and the cast iron chips in the heat-treatment container, induces the formation of aluminate spinel,

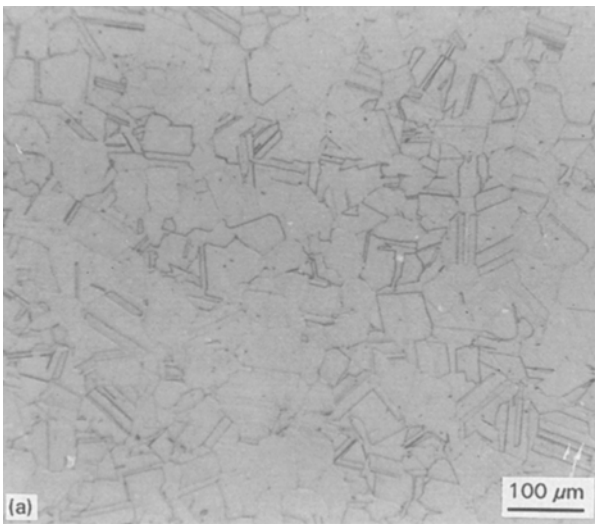

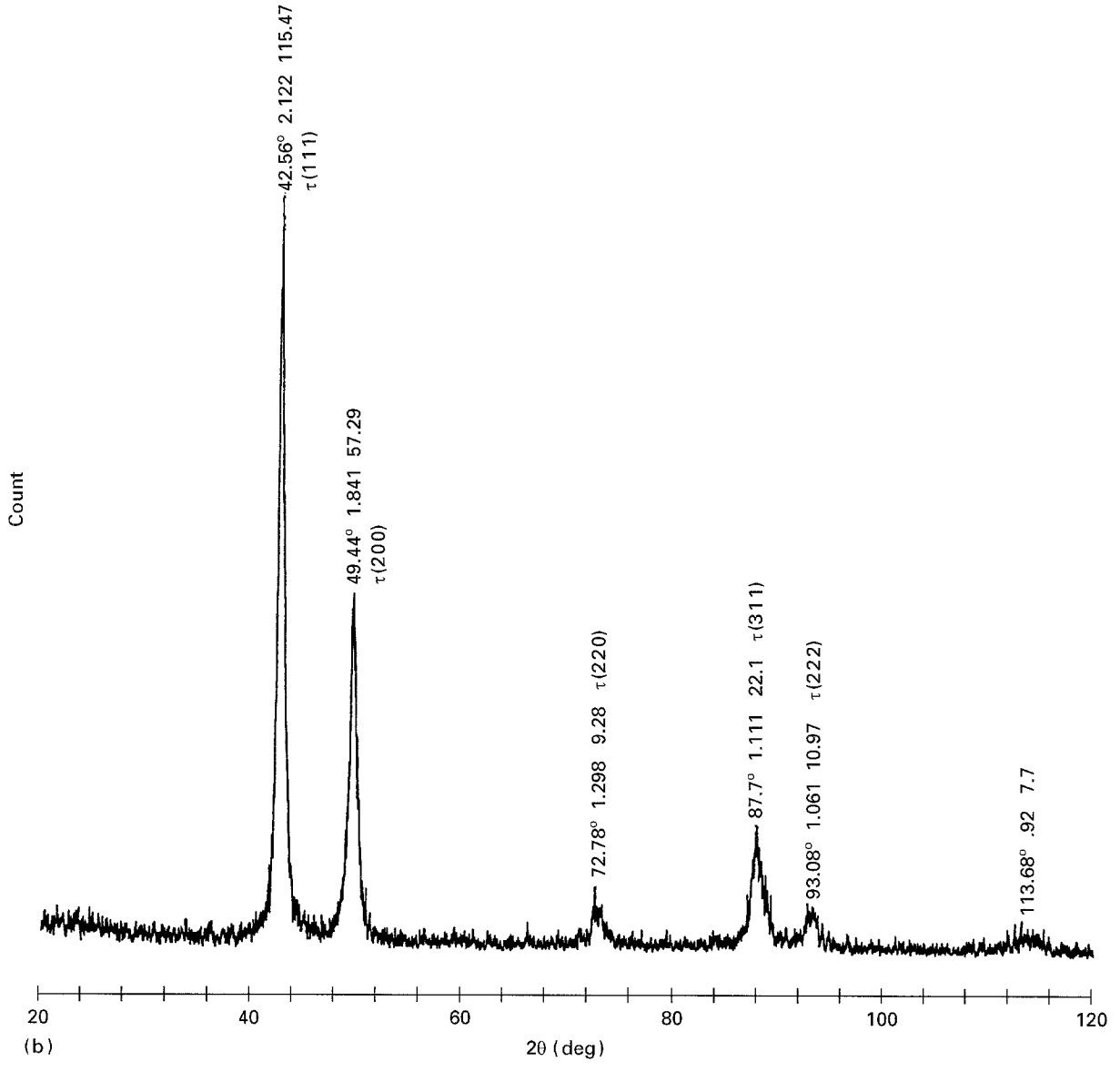

Figure 2 (a) Photograph of the typical bulk structures of the alloy after the final annealing treatment. (b) X-ray diffraction pattern of structure shown in Fig. 2a.

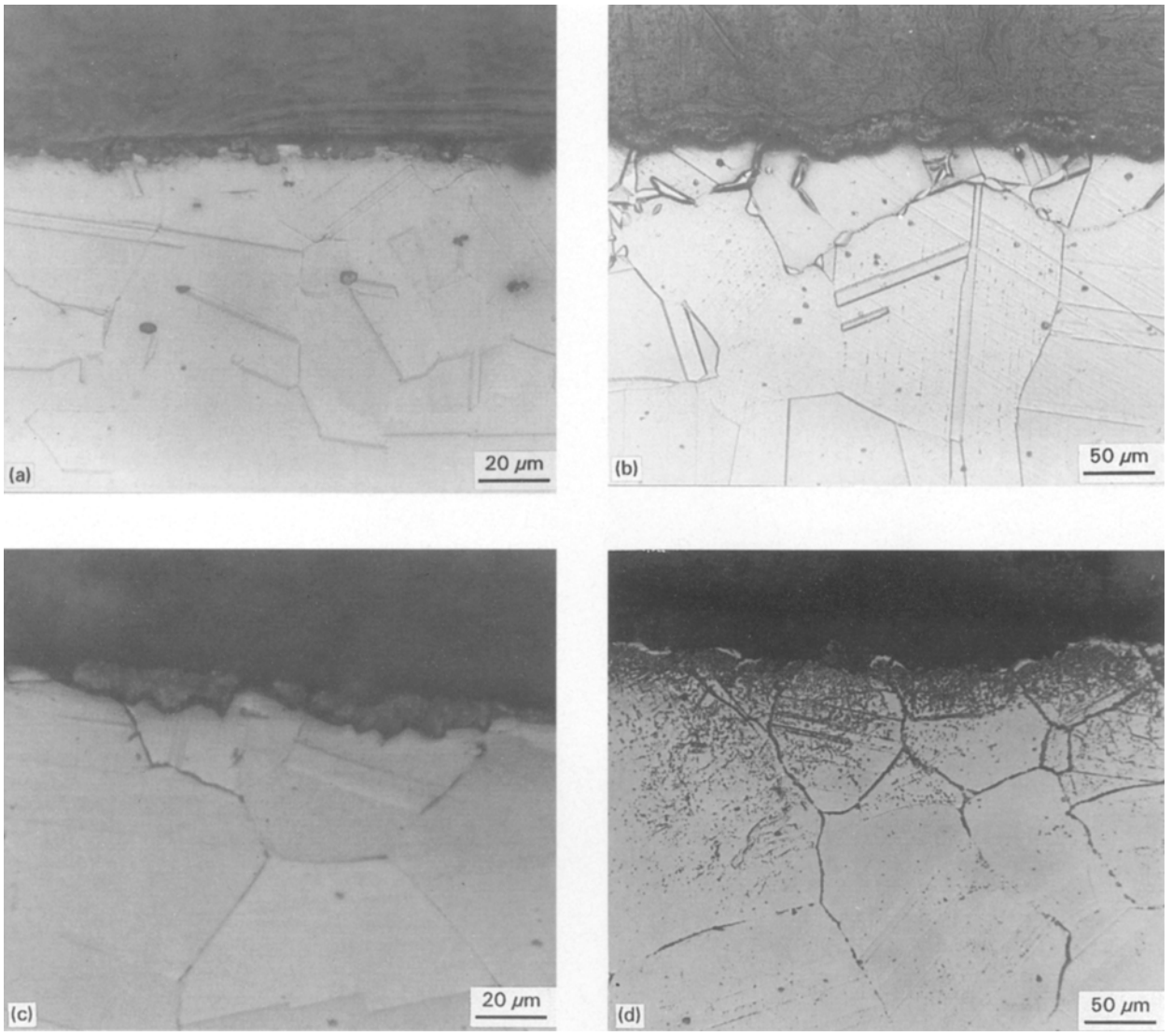

Figure 3 The surface microstructure of the alloy treated by G, G1 and G2. (a) Thin black scale observed on the surface of the alloy treated by the G process. (b) Small ferrite grains of the alloy treated by the G2 process. (c) Surface microstructure of the alloy treated by the G1 process, in which the heat-treatment container is filled with cast iron chips. (d) Surface microstructure of the alloy treated by the G1 process, in which air and cast iron chips coexisted in the heat-treatment container; a needle-like structure and coarse grain boundary are observed.

TABLE I Tensile properties of the alloy treated by G, G1, and G2 processes.

Heat treatment	Yield strength (MPa)	Tensile strength (MPa)	Elongation (%)
G	772.36	1013.89	54.41
G1	$\leqslant$ 672.11	846.38–916.3	16.85–55.1
G2	655.87	821.93	64.23

aluminium nitride nodules and grain boundary oxide on the alloy, as indicated in Figs 3, 5 and 6. These oxides embrittle this alloy severely, as shown in Table I. A similar oxidation phenomenon has been observed on the Ni–Cr and Ni–Cr–Fe alloys heated in carbon-containing gas and this phenomenon was named "green rot" [26]. The overall oxidation process involved internal carburization of Cr (apparently along grain boundaries) followed by oxidation of carbide particles. The internal carburization severely embrittled those alloys. The similarity between the degradation phenomenon of this alloy and the Ni–Cr–Fe alloys in the carbon-containing atmosphere makes it reasonable to propose that degradation of this alloy is accomplished by the "green rot" attack process. Since there is a tendency for aluminium carbide formation in FeMnAl alloy [27, 28], the enrichment of Al and Si in the grain boundary oxide implies that Al and Si are the carburized elements of this FeMnAlSi alloy when it is heated in the carbon-containing atmosphere. This phenomenon has not been observed and reported before.

Since the annealing temperature and time interval of the G1 and G2 processes are the same, the fact that no oxide nodule is observed on the specimen annealed by G2 process implies that the carbon-containing gas enhances the oxidation rate of the alloy studied. The appearance and structure of the oxide nodules are similar to those observed on a FeMnAl alloy heated in air at 1000 °C for 24 h [9].

The strength of this alloy treated by the G1 process is 3–11% greater than that treated by the G2 process. This might be due to the different diffusion direction of the carbon atoms in these two treatment

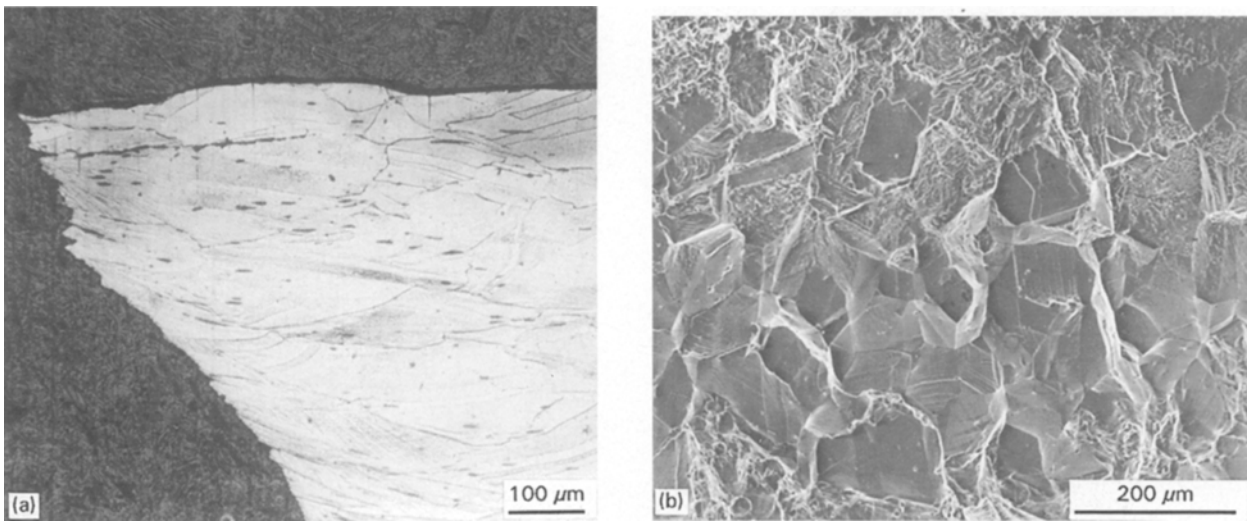

Figure 4 Cracking path and fracture surface of specimen treated by the G1 process. (a) The fracture surface of the specimen with the needle-like structure. (b) Cracking path of the specimen without the needle-like structure.

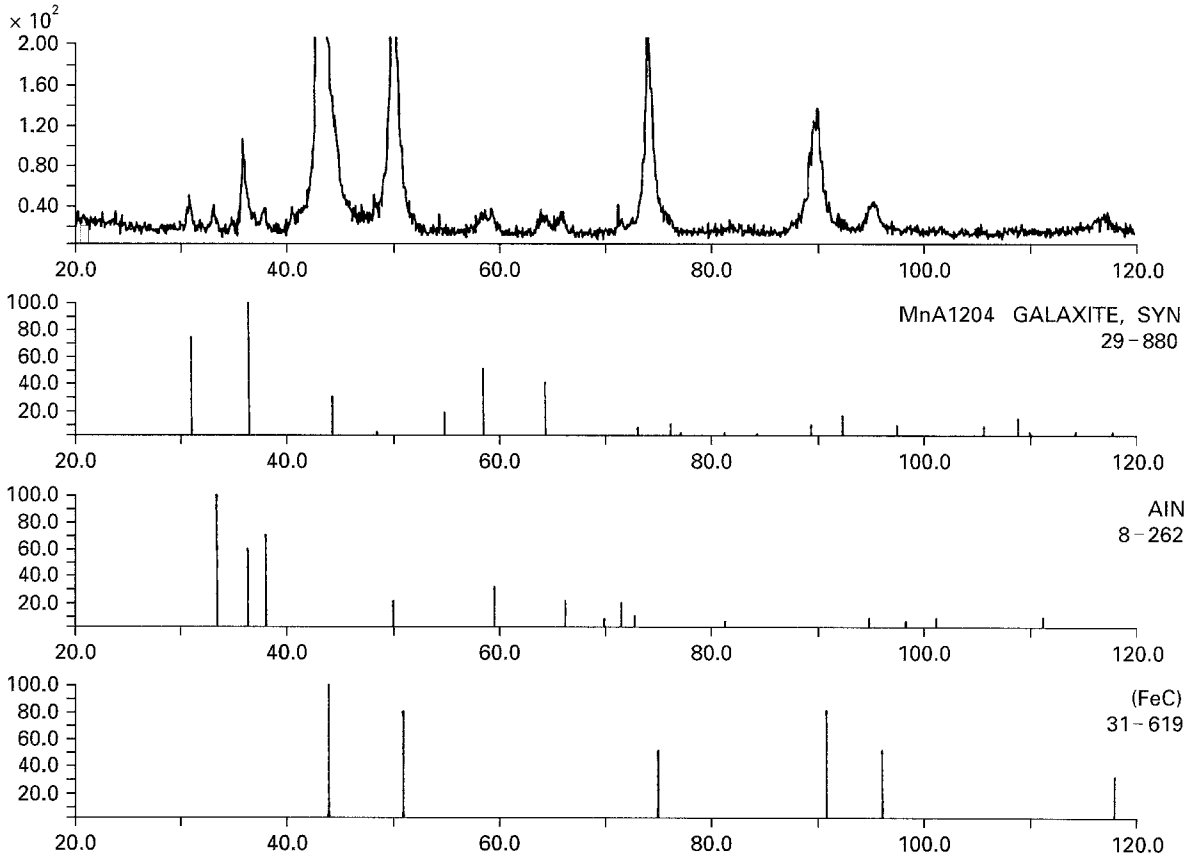

Figure 5 The X-ray diffraction pattern of the needle-like structure. The needle-like structure is shown to be a mixture of $MnAl_2O_4$ and AlN.

environments. In the carbon-containing atmosphere, the direction of carbon diffusion was into the alloy because of the carbon-rich environment. The inward diffusion of carbon atoms increased the alloy's strength and decreased its elongation. The tensile strength of this alloy treated by the G process is higher than that of those alloys treated by the other two processes. The highest tensile strength comes from the grain size effect. The grain diameter of the alloy treated with the G process is about one third of that treated by the other two processes. Since the strength of the alloy is proportional to the reciprocal of the square root of the grain diameter, the alloy treated by the G process certainly has the highest tensile strength.

5. Conclusions

1. Surface oxide nodules and grain boundary oxide were found to form on Fe–32Mn–9.4Al–lC–1.27Si alloy when it was annealed in a carbon containing atmosphere at 1050 °C for 1 h. This oxidation reaction was thought to be the result of the "green rot" attack process as observed on Ni–Cr–Fe alloys.

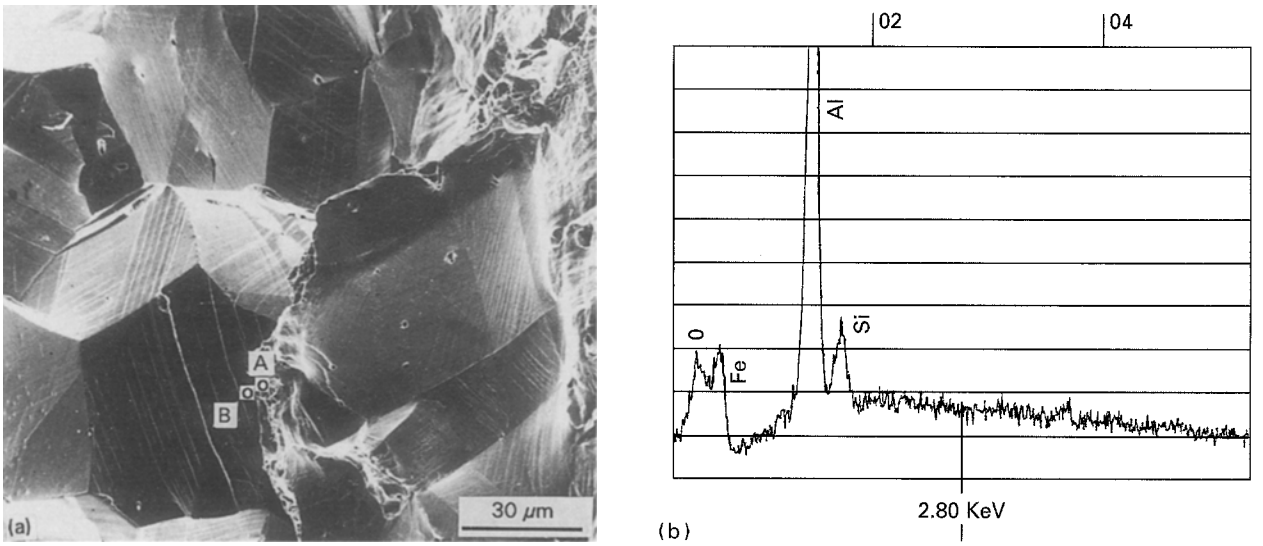

Figure 6 (a) Locations of EDS analysis. (b) EDS spectrum of the coarse grain boundary as shown in Fig. 6a, point A.

2. The carbon-containing gas generated by the co-existence of air and cast iron chips enhanced the oxidation rate of the Fe–32Mn–9.4Al–1C–1.27Si alloy at 1050 °C.

3. This carbon-containing atmosphere embrittled the Fe–32Mn–9.4Al–1C–1.27Si alloy through the internal carburization and oxidation process.

Acknowledgement

This work was supported by the National Science Council, Republic of China under Grant NSC-81-0405-E-007-556.

References

1. S. K. BANERJI, *Met. Prog.* **122** (1978) 59.
2. J. CHARLES, A. BERGHEZAN, A. LUTTS and P. L. DANWISNE, *ibid.* **123** (1981) 71.
3. J. B. DUH, W. T. TSAI, and J. T. LEE, *Scripta Metall.* **21** (1987) 95.
4. G. E. HALE and A. J. BAKER, in "Alternate alloying for environment resistance", edited by G. R. Smolik and S. K. Banerji (American Institute of Mining, Metallurgical and Petroleum Engineers, Warrendale, PA, 1987), p. 67.
5. R. K. YOU, P. W. GAO and D. GAN, *Mater. Sci. Eng.* **A117** (1989) 141.
6. J. P. SAUER, R. A. RAPP and J. P. HIRTH, *Oxid. Met.* **18** (1982) 285.
7. P. R. S. JACKSON and G. R. WALLWORK, *ibid.* **21** (1984) 135.
8. C. H. GAO, PhD thesis, National Tsing Hua University, Hsinchu, Taiwan (1987).
9. C. J. WANG and J. G. DUH, *J. Mater. Sci.* **23** (1988) 769.
10. J. J. CHAN and S. C. CHANG, *ibid.* **25** (1990) 1331.
11. M. CAVALLIN, F. FELLI, R. FRATESI and F. VENIALL, *Werkstoffe und Korrosion* **33** (1982) 281.
12. R. WANG and F. H. BECK, *Met. Prog.* **125** (1983) 72.
13. C. J. ALSTETTER, A. P. BENTLEY, J. W. FOURIE and A. N. KIRKBRIDE, *Mater. Sci. Eng.* **82** (1986) 13.
14. S. C. TJONG, *Werkstoffe und Korrosion* **37** (1986) 444.
15. R. WANG and G. R. WALLWORK, in "Alternate alloying for environment resistance", edited by G. R. Smolik and S. K. Banerji (American Institute of Mining, Metallurgical and Petroleum Engineers, Warrendale, PA, 1987) p. 306.
16. J. B. DUH, W. T. TSAI and J. T. LEE, *Corrosion* **44** (1988) 810.
17. S. T. SHIH, C. Y. TAI and T. P. PERNG, *ibid.* **49** (1993) 130.
18. D. J. CHAKRABARTI, *Metall. Trans.* **8B** (1977) 121.
19. T. F. LIU and C. M. WAN, *Scripta Metall.* **19** (1985) 805.
20. K. H. HWANG, W. S. YANG, T. B. WU, C. M. WAN and J. G. BYRNE, *Acta Metall.* **39** (1991) 825.
21. A. P. BENTLEY, J. W. FOURIE and C. J. ALSTETTER, in "Alternate alloying for environment resistance", edited by G. R. Smolik and S. K. Banerji (American Institute of Mining, Metallurgical and Petroleum Engineers, Warrendale, PA, 1987) p. 377.
22. M. T. JAHN, J. J. CHAN, C. H. GAO, C. M. WAN and S. C. CHANG, "Alternate Alloying for Environment Resistance", edited by G. R. Smolik and S. K. Banerji (AIME, 1987), p. 179.
23. S. C. CHANG, T. S. SHEU and C. M. WAN, in Proceedings of the 7th International Conference on Strength of Metals and Alloys, Montreal, Canada, August 1985, edited by H. J. McQueen, J. P. Bailon, J. I. Dickson, J. J. Jonas and M. G. Akben (Pergamon, Oxford, 1985) p. 1081.
24. J. C. GARCIA, N. ROSAS and R. J. RIOJA, *Met. Prog.* **124** (1982) 47.
25. H. ERHART, R. WANG and R. A. RAPP, *Oxid. Met.* **21** (1984) 81.
26. P. KOFSTAD, "High temperature corrosion" (Elsevier Applied Science, London and New York, 1988) p. 534.
27. M. V. C. ARABE and E. M. P. SILVA, "Alternate alloying for environmental resistance", edited by G. R. Smolik and S. K. Banerji (American Institute of Mining, Metallurgical and Petroleum Engineers, Warrendale, PA 1987) p. 448.
28. S. C. TJONG and N. J. HO, *Mater. Sci. Eng.* **90** (1987) 161.

Received 14 February 1994
and accepted 1 December 1995